Rev. Adv. Mater. Sci. 44 (2016) 407-419

MAGNETIC PROPERTIES OF NICKEL DOPED TITANIUM DIOXIDE: A CASE OF Ni,N-TiO_2 NANOCOMPOSITES

J. Typek[1], N. Guskos[1], G. Zolnierkiewicz[1], S. Mozia[2] and A.W. Morawski[2]

[1]Department of Physics, West Pomeranian University of Technology, Al. Piastow 48, 70-311 Szczecin, Poland
[2]Department of Chemical and Environmental Engineering, West Pomeranian University of Technology, Al. Piastow 17, 70-310 Szczecin, Poland

Received: December 11, 2015

Abstract. In the first part of this article a review of relevant papers dealing with the magnetic properties of nickel doped titanium dioxide is presented. Each paper is shortly described, including information about sample preparation method, used magnetic detection techniques, and the main results from the investigated materials. A short summary of the reviewed papers is presented and the main ideas relevant to the room temperature ferromagnetism (RTFM) observed in many samples of Ni:TiO_2 are discussed and possible mechanisms of RTFM are formulated. In the second part, the investigations of nickel and nitrogen co-modified titanium dioxide nanocomposites, *n*Ni,N-TiO_2 (where *n* = 1, 5, and 10 wt.% of Ni), by dc magnetisation measurements in 2-300K range and in external magnetic field up to *H*=7 T, are presented. Complex magnetic behavior of the studied nanocomposites has been revealed. The samples showed weak ferromagnetism with Curie temperature above room temperature. No superparamagnetic behavior was registered in the studied temperature range. Comparison of the obtained magnetic parameters (saturation magnetisation, remanent magnetisation and coercive field) of *n*Ni,N-TiO_2 with previously studied similar nanocomposites, *n*Fe,N-TiO_2 and *n*Co,N-TiO_2, is presented and the conclusions about the nature of their ferromagnetism are drawn. Small value of Ni magnetic moment indicate that RTFM in *n*Ni,N-TiO_2 nanocomposites originate mostly from metallic nickel nanoparticles.

1. INTRODUCTION

Titanium dioxide (TiO_2) is the most widely used semiconductor-based heterogeneous photocatalyst. This material is nontoxic, cheap, resistant to photo-corrosion, and has a high oxidative power. It permits the sunlight to be used for the destruction of toxic pollutants, allows selective redox transformations in certain organic compounds, is used in production of hydrogen, and is applied in the conversion of solar energy to electric power [1-4]. One important disadvantage of this material for photocatalysis is its wide band gap (above 3 eV) that prevents an effective absorption of the visible part of the solar radiation. To remedy this drawback TiO_2 was doped with both transition metal (e.g. Fe, Co, Ni, Cr, Cu, V) and non-metal (e.g. N, S, C, B) impurities [5]. On one hand doping had decreased the photothreshold energy for TiO_2 but on the other hand it also reduced its overall activity through introduction of recombination centres for electrons and holes. Doping also brought one unexpected result as their magnetic properties are concerned – TiO_2 showed ferromagnetism (FM) at room temperature (RT).

The first report on room temperature ferromagnetism (RTFM) in TiO_2 thin films was published in 2001 [6]. Since the discovery of Matsumoto *et al*., a lot of research has been carried out on RTMF in TiO_2 samples having different forms (thin films, nanopowders, nanocrystals, nanorods, etc.). The

Corresponding author: J. Typek, e-mail: typjan@zut.edu.pl

main reason of such an enormous interest followed from the potential wide applications of these materials in microelectronic devices based on the spin degree of freedom of an electron (spintronics). Earlier theoretical works indicated that the introduction of Mn into GaN, GaP as well as ZnO and other oxide materials could produce RTFM [7]. The proposed model, called the free carrier mediated exchange model, explained the FM by the exchange interaction between carriers and the localized spins i.e. the magnetic property was mediated by the charge carriers of the materials. Unfortunately, this model can be applied only to materials having high hole concentrations and thus is not suitable for low carrier concentrations. The double exchange mechanism model is more suitable in that case [8]. It puts forward the idea that magnetic ions in different charge states couple with each other by virtual hopping of an extra electron from one ion to the other. In effect, the 3d electron in the partially occupied 3d orbitals of the metal ion is allowed to hop to the 3d orbitals of the neighbouring metal ion, provided that they have parallel magnetic moments [9]. In yet another model proposed by Coey et al. the FM exchange is mediated by shallow donor electrons that form bound magnetic polarons (BMP), which in turn overlap to create a spin split impurity band. Magnetic ions in different charge states are coupled by virtual hopping of the 'extra' electron from one ion to the other [10]. Since that time many papers have been devoted to the subject of the so-called diluted magnetic semiconductors (DMS) in which non-magnetic semiconductors are doped with magnetic atoms [11]. Typical DMS oxides are ZnO, In_2O_3, TiO_2, SnO_2, CuO, and HfO_2 [12]. The subject of DMS is still very controversial. Numerous reports have ascribed the RTFM to intrinsic causes, while a large number of others attributed these RT magnetic effects exclusively to impurities. Thus the observed RTFM phenomenon in insulating samples is still a challenge both for experimentalists and materials science theorists.

The reason for the broad interest in DMS lies in their potential applications in spin electronics (spintronics). It is expected that DMS will be the future solution to downsize the current microelectronic devices into the size of even nanometers [13,14]. DMS materials offer the control of charge carrier spin to carry information and they can be used in such devices as e.g. spin valves, spin transistors and spin light emitting diodes (LEDs). A spin valve is a device which utilizes the giant magnetoresistive effect, it functions by alternating its electrical resistance depending on the alignment of the magnetic layers. The device can be made highly resistive or highly conductive depending on the direction of the applied magnetic field in the conducting layers. Spin transistors are similar to typical metallic semiconductor transistors, and may function as switches or amplifiers, or for data storage. A spin transistor is a device which uses the fact that electrons exist in one of two spin states, spin up or spin down. The electrons are set in a particular spin state to store information, for example spin up and spin down being analogous to a 1 and a 0 in binary numbering. A LED functions similar as typical semiconductor-based LED, with the additional advantage of controlling the spin state. LEDs function by injection of a charge carrier, usually an electron, from a ferromagnet into a semiconductor layer where it combines with a hole supplied by the substrate, resulting in the emission of light. The emitted light will then have a polarization depending on the spin-polarization of the charge carriers involved in the recombination. Although a lot of important discoveries concerning useful properties of DMS in applications in spintronic devices have been published, there is still need for further investigations with variety of characterisation techniques, especially including measuring the number and type of free carriers. This will clarify the nature of the FM phenomenon in these very interesting materials and make it controllable so that it can be more easily incorporated into device structures.

In this article a review of papers devoted to the magnetic investigation of Ni doped TiO_2 will be presented first, followed by the description of a new magnetic results concerning nickel and nitrogen co-modified titanium dioxide nanocomposites (*n*Ni,N-TiO_2). The obtained magnetic characteristics for Ni,N-TiO_2 nanocomposites with different concentrations of nickel dopant (*n*=1, 5, and 10 wt.%) will be compared with previously acquired similar data for *n*Fe,N-TiO_2 and *n*Co,N-TiO_2 nanocomposites and conclusions will be drawn on their magnetic structure and magnetic interactions in these systems.

2. REVIEW OF MAGNETIC INVESTIGATIONS OF NICKEL DOPED TITANIUM DIOXIDE

In Table 1, the relevant information on the published papers that deal with magnetic characterization of nickel doped titanium dioxide, is presented [15-42]. Three important features of the presented papers (column 1) are selected and described: sample preparation method and the obtained sample structural properties (column 2), the used magnetic de-

Table 1. Review of papers devoted to magnetic characterisation of nickel doped TiO_2.
The following abbreviations are used: FM – ferromagnetic, ferromagnetism; RTFM – room temperature ferromagnetism; PM – paramagnetic, paramagnetism; SPM – superparamagnetic, superparamagnetism; H_c – the coercive field; M_s – saturation magnetisation; T_b –the blocking temperature; NP – nanoparticle; OV – oxygen vacancy; EPR – electron paramagnetic resonance; FMR – ferromagnetic resonance; ZFC – zero field cooling; FC – field cooling.

Ref.	Samplepre paration method and structural properties	Detection method	Main conclusions about magnetic properties
15	Thin films grown by the laser ablation on $LaAlO_3$ and $SrTiO_3$ substrates	• SQUID magnetometry	• FM is not due to Ni segregations but due to Ni:TiO_2 matrices
16	Magnetic Ni NP (3-18 nm) embedded in TiO_2 single crystals synthesized by ion implantation	• SQUID magnetometry; *M(H)*, *M(T)* in FC/ZFC modes	• H_c of Ni NPs was about 210 Oe at 10 K • T_b was about 85K
17	Thin films grown by a pulsed laser deposition technique on $LaAlO_3$, $SrTiO_3$ and silicon substrates, 4.3% of Ni	• SQUID magnetometry; *M(H), M(T)* • Magnetic force microscopy at RT	• RTFM does not stem from any kind of dopant clusters • Magnetic moment strongly depends on growth temperature
18	Single crystals of TiO_2 rutile implanted with high fluence of Ni ions	• SQUID magnetometry; *M(H)*, *M(T)*	• ZFC magnetisation displays SPM behaviour with T_b= 50K • Nanometric sizes of Ni metallic clusters
19	Ni nanocrystals with 3–20 nm in dimensions embedded in TiO_2 rutile matrix synthesized by ion beam implantation	• SQUID magnetometry; *M(H)*, *M(T)*	• SPM Ni NPs with T_b= 85K • H_c of Ni NPs was about 210 Oe at 10K • The mean-magnetic moment per MP calculated from Langevin fitting was 11064 μ_B
20	Single crystals of TiO_2 rutile doped with Ni (0.41%) in form of elongated needles grown with the flux method	• SQUID dc magnetometry; *M(T), M(H)* at RT	• Superposition of FM and PM behaviour observed at RT • Only a small fraction of ions is involved in FM ordering at RT
21	Single crystals of $Ti_{1-x}Ni_xO_2$ (x = 0.0008) with rutile structure grown by floating zone method	• SQUID magnetometry *M(H)*, *M(T)*	• FM can be observed in crystals grown in a pure nitrogen gas, while only weak PM can be found even at 4K in crystals grown in a pure oxygen gas • Inhomogeneous model of magnetism that assumes FM domains imbedded in PM matrix
22	Thin films grown by sol-gel method deposited on Al_2O_3, nickel concentrations up to 9 at.%	• Vibrating sample magnetometry • SQUID magnetometry	• A higher Ms [m_B/Ni] is obtained for a lower dopant concentration (x<6 at.%) • Metallic clusters form for x>6 at.% • RTFM involves localized (by OV) electrons
23	Thin films epitaxially grown by reactive magnetron sputtering on SiO_2 substrates	• Vibrating sample magnetometry • Magnetic force microscopy	• Thin films show FM at RT • Magnetic moment per Ni increases with Ni concentration up to 8% • Magnetic domains are homogeneous, have regular shapes • FM originate from doped matrix and OVs play important role

24	TiO_2 with 5 at.% Ni obtained by thermal treatment	• Vibrating sample magnetometry *M(H)* at RT, AC susceptibility *M(T)*	• FM due to unreacted Ni atoms • Magnetic moment (0.67 μ_B/Ni) lower than in thin films
25	Needle-shaped rutile crystals (Ni<0.5%) grown by flux method	• EPR • SQUID magnetometry *M(T)* and *M(H)*	• No EPR signal from Ni • Prevailing PM response with a weak FM contribution • RTFM is connected with non-homogenously diluted Ni in TiO_2 matrix together with free charges related to oxygen sub-stoichiometry.
26	Theoretical paper	• Calculations using series of supercell density functionals	• OVs plays a key role of FM in Ni-doped TiO_2, and the magnetic origin is of Ni^{3+} ion • A vacancy-mediated direct-exchange mechanism is proposed
27	Nanobelts with different Ni^{2+} contents prepared by combining ion exchange with hydrothermal treatment	• SQUID magnetometry; *M(H)* loops at RT	• Dominating PM response with a weak FM contribution at RT
28	Theoretical paper: Ni doped anatase TiO_2	• The calculations performed with the local spin density approximation based on density functional theory	• Electronic structure calculated • PM ground state for nickel doped anatase
29	Ni-implanted rutile single crystals subjected to different annealing	• SQUID magnetometry; *M(T)* in ZFC/FC modes and *M(H)* loops	• FM is due mostly to metallic nickel nanocrystals • Nanocrystalline size increased with annealing temperature • T_b increased with annealing temperature
30	Ni-doped (up to 10 at.%) TiO_2 NPs synthesized by the non-hydrous complex-polymer sol–gel method	• SQUID magnetometry; *M(T)* in ZFC/FC modes and *M(H)* loops	• Samples mostly PM • The presence of $NiTiO_3$ with an AFM peak at 23K • SPM component from NiO NP (12 nm)
31	0.05 and 0.5 mol.% Ni-doped TiO_2 powders prepared by a modified sol–gel route	• Vibrating sample magnetometer; *M(H)* at RT • Magnetic force microscopy	• 0.5 mol.% Ni:TiO_2 is PM, 0.05 mol.% Ni:TiO_2 is FM • FM from the spin ordering through exchange interaction between holes trapped in oxygen 2p orbital adjacent to Ni_{Ti} site and its propagating influence through hole mediation
32	Single crystal rutile TiO_2 with unintentional Ni contamination	• SQUID magnetometry; *M(H)* loops	• Segregated surface layer of Ni gives rise to the observed FM • Under vacuum annealing Ni segregates to the surface over a 50 nm layer where the Ni concentration exceeds 10%–20% and drops with subsequent air annealing
33	Ni-doped TiO_2 films deposited on Si substrates by sol–gel technique	• Vibrating sample magnetometry at RT, *M(H)* loops	• Important role of anatase-rutile junction • FM-PM-FM properties with Ni concentration increase • F-centre bound magnetic polaron as a possible source of FM

34	Nanowires synthesized by solvothermal method.	• Vibrating sample magnetometer at RT, *M(H)* loops	• Surface defects such as Ti^{3+} and OVs play more important role in realizing RTFM than Ni doping • Undoped TiO_2 nanowire shows RTFM • M_s increases with Ni doping (up to 5 at.%)
35	TiO_2 films deposited on Si substrates by a sol–gel process	• Vibrating sample magnetometer at RT, *M(H)* loops	• Magnetisation of doped samples decrease with increasing metal element contents • Magnetic properties may be related to the influence of the anatase-rutile transformation on the magnetic polarons
36	Nanorods (diameter 80-120 nm) synthesized from anatase TiO_2 and Ni nitrate by one-step hydrothermal reaction	• Vibrating sample magnetometer, M(H) loops at RT • EPR spectrometry	• FM at RT • Ni atoms are incorporated into the titanate lattice
37	Ni doped (2-10%) anatase TiO_2 NPs prepared by sol-gel method (sizes 7.3-8.3 nm)	• ESR spectroscopy • SQUID magnetometry, *M(H)* loops at 5 K	• PM behaviour • No EPR signal from nickel
38	Ni^{2+} (up to 1.8 at.%) doped TiO_2 NPs (15-20 nm) synthesized by shape transformationof titania nanotubes in the presence of Ni^{2+} ions, as precursors, in extended hydrothermal treatment	• SQUID magnetometry, *M(H)* loops	• Weak FM at RT in all samples • No metallic Ni and no clustering of Ni • M_s decreases on increasing Ni content • The super-exchange d–d interaction between the neighbouring atoms is not responsible for the observed RTFM • OVs play a role of mediator of exchange interaction between magnetic dopant atoms
39	Ni doped (8 wt.%) titanate nanotubes with outer and inner diameters of ten and six nm synthesized via thehydrothermal method	• Vibrating sample magnetometer at RT • SQUID magnetometry, *M(H)* at 40K, *M(T)*	• Dopant Ni atoms exist as a trivalent species, which interact with H^+ in the nanotubes' interlayers. • Weak SPM effect is due to the interacting spins with relatively larger Ni-doped nanotubes • FM is due to interaction of Ni^{3+} with titanate's 3d electrons
40	Ni doped (3 and 6 mol.%) TiO_2 by sol-gel method, NPs sizes 30-40 nm	• Vibratingsample magnetometer, *M(H)* loops at RT	• M_s increases with concentration increase, but M_r and H_c decrease (because of more PM $NiTiO_3$) • FM is due to the carriers exchange coupling
41	Nickel (1, 5, 10 wt.%) and nitrogen co-modified TiO2 prepared by impregnation of amorphous titanium dioxide	• EPR/FMR spectroscopy in 4-290K range	• Broad FMR lines in 4-290 range and narrow EPR lines attributed to Ti^{3+} on grains' surface • FMR line decomposed on three components: one from metallic Ni clusters, two from Ni in TiO_2 lattice
42	Theoretical paper; rutile $Ti_{0.75}Ni_{0.25}O_2$	• Density functional theory with the plane wave self-consistent field method	• Magnetic properties can be explained by spin polarization of d states of Ti with dopants

tection methods (column 3), and the main conclusions concerning magnetic properties of the studied samples (column 4). As it can be read from column 2, the following sample forms of Ni:TiO_2 were produced: thin films [15,17,22,23,33,35], crystals and nanocrystals [16,18-21,25,29,32], nanopowders [24,30,31,37,38,40,41], nanobelts [27], nanowires [34], nanorods [36], and nanotubes [39]. The content of nickel in different samples varied – from negligible to up to 10 at.% (nominally, but actually probably much smaller). The methods of sample synthesis were also very different, depending on the required final form of the sample. In case of thin films, laser ablation on different substrates, pulsed laser deposition, sol-gel method, and epitaxy by reactive magnetron sputtering, were applied. Crystals and nanocrystals were synthesized by nickel implantation of crystals, grown by floating zone method, by flux method, or by using unintentional contamination by Ni ions of TiO_2 single crystals. Nanopowders were mostly produced by different variations of sol-gel and hydrothermal methods. Nanobelts, nanowires, nanorods and nanotubes were synthesized by ion exchange combined with hydrothermal treatment, by solvothermal method, and by hydrothermal reaction.

It is well known that TiO_2 has three main polymorphs found in nature: rutile (tetragonal), anatase (tetragonal), and brookite (orthorhombic). However, only two former phases play any role in the applications of TiO_2. The thermodynamically favourable phase is rutile with 6 atoms in the units cell forming a slightly deformed octahedron. Anatase TiO_2 has also the tetragonal crystal structure, but its octahedron is more deformed in comparison to rutile phase. After the TiO_2 nanoparticles reach a certain size (depending on preparation method, a crossover size is roughly 30 nm) anatase phase transforms to rutile structure which becomes prevailing for larger nanoparticles. Also the heat treatment during synthesis of particles plays a vital role in this phase transformation. An anatase to rutile phase transformation undergoes usually in the range from 600-700 °C, but it is influenced by preparation conditions, impurities, precursors, oxygen vacancies, particle sizes etc. It has been reported that this transformation temperature is increased by dopants such as Si, Al, and Zr, while it is decreased by addition of Co, Mn and V. Most samples listed in Table 1 has a rutile structure with exceptions of nanorods [36] and nanopowders [37]. In Ref. [33] an important role of the anatase-rutile junction, in creating magnetic properties of these materials, was stressed [33]. They noticed that with increasing concertation of Ni, the anatase phase diminishes and for Ni content of 7 mol% only the rutile phase survives. The anatase-rutile junction can effectively destroy magnetic polaron (by separating the carriers) and thus to diminish magnetic property of Ni:TiO_2. In addition, the higher the Ni concentration, the smaller the number of oxygen vacancies [33].

The role of oxygen vacancies in modifying the magnetic properties of doped TiO_2 is not to be underestimated [43]. When Ti^{4+} site is substituted by Ni^{2+}, two oxygen defects are also introduced. These vacancies can trap carriers. As TiO_2 shows a strong polaronic effect due to strong electron–phonon interactions, a polaronic electron will be trapped near the vacancy and form an F-centre. The trapped electron orbital has a large radius and can overlap the d orbitals of the neighbouring magnetic ions. Consequently, a possible origin of FM in TiO_2 doped with magnetic ions is an F-centre bound magnetic polaron (BMP), which is formed by an electron trapped in an oxygen vacancy and neighbouring magnetic doped ions. It should be also remembered that as oxygen vacancies can be easily generated by annealing in oxygen-deficient environments, annealing temperature and annealing atmosphere can play an important role in magnetism of these materials. Annealing temperature has an effect on the crystal structure of TiO_2 (rutile or anatase) as well on an average size of nanoparticles. Higher annealing temperature can also influence the phase content of sample, e.g. new phases involving doped ions may be formed.

In column 3 of Table 1, the detection methods used in study of magnetic properties of Ni:TiO_2 samples are presented. These are: dc and ac magnetometry using SQUID or vibrating sample magnetometer, magnetic force microscopy and electron paramagnetic resonance/ferromagnetic resonance (EPR/FMR) spectroscopies. Typical magnetic characterisation done by magnetometers include measurements of temperature dependence of magnetic susceptibility $\chi(T)$ (where $\chi = M/H$), and isothermal magnetization *M(H)* in form of a magnetic loop in case of FM material. Often the existence of superparamagnetic (SPM) phase is detected in comparing *M(T)* dependence registered in ZFC (zero field cooling) and FC (field cooling) modes. Temperature, at which *M(T)* curve in ZFC mode reaches a maximum, is called the blocking temperature T_b. Magnetic force microscopy can be used to obtain magnetic scans of material surface and thus identify e.g. domain walls or metallic clusters. Magnetic resonance spectroscopy in form of EPR or FMR variants can detect the presence of small amounts

of paramagnetic phases or impurities as well as FM nanoparticles or clusters and help understand their dynamics.

In column 4 of Table 1 the main conclusions reached in each paper are listed. The main question the authors try to answer is whether a specific sample is FM at RT and if so what is the mechanism that produces FM at that high temperature. Most of the synthesized Ni:TiO_2 samples displayed FM at RT [e.g. 15,22,24,29,36,38], but few samples were only paramagnetic (PM) or SPM [e.g. 25,27,30,37]. Such a broad spectrum of magnetic behaviour shouldn't be surprising taking into account a large number of samples synthesized by using so much different techniques and very different preparatory conditions. What's more a given sample can be magnetically inhomogeneous and be partially FM, and in part PM, SPM or AFM [20,30]. Because so many factors have a crucial influence on the magnetic state of Ni:TiO_2, it can be impossible to present one coherent picture of FMRT in these materials. To the list of the most important factors that shape the magnetic characteristics the following may be counted: the type of crystal structure of TiO_2 (anatase or rutile), the presence of anatase-rutile junction, the presence of oxygen vacancies, the growth temperature, the annealing temperature, the annealing atmosphere (oxygen, vacuum), the content and distribution of Ni dopant, the presence of secondary phases, the sizes of nanoparticles.

The most important question related to RTFM in Ni:TiO_2 is whether the FM originates from intrinsic (i.e. mediated by carriers or intentional defects inside the host semiconductor) or extrinsic (e.g. native or dopant-introduced defects, formation of FM secondary phases, metallic clusters) causes. This question is especially difficult to answer in case of magnetic dopants like Ni, Fe, and Co, which are FM in nature. As a matter of fact RTFM might be originating from both types of causes in Ni:TiO_2 system, even in the same sample at the same time. Wheatear intrinsic or extrinsic cause is realized in particular sample depends on the above mentioned factors. Extrinsic origin of RTFM (metallic clusters) can be identified from magnetic measurements by calculation of the magnetic moment per single Ni atom (from the saturation magnetisation M_s derived from hysteresis loop) or by observation of the temperature dependence of magnetization in ZFC and FC modes. For metallic Ni clusters the magnetic moment per single Ni atom should be similar to what is obtained for pure bulk Ni metal (0.61 μ_B/Ni). On the other hand, for Ni^{2+} in octahedral complexes, experimentally observed spin-only magnetic moment is in 2.9-3.3 μ_B/Ni range. If Ni metal cluster can be treated as a magnetic nanoparticle suspended in TiO_2 matrix, SPM behaviour is expected and can be registered in $M(T)$ dependence in ZFC mode as magnetisation maximum at the so-called blocking temperature T_b. From T_b value the size of a nanoparticle can be estimated (the bigger the particle, the higher the blocking temperature).

The most popular model of RTFM in transition metal doped TiO_2, treating it as an intrinsic effect, was proposed by Coey et al. [10]. It is a donor impurity band model which is the extension of the BMP model, to describe the properties of defect (e.g. oxygen vacancies) derived n-type dilute magnetic oxides. Oxides are n-type, due to oxygen vacancies, and have a high dielectric constant. Shallow donors are associated with defects form BMPs, via which FM ordering of magnetic moments of dopants is mediated. At a sufficiently high BMP concentration, the polarons overlap, thus leading to a spin-split impurity band in the band gap and FM ordering throughout the material follows. Although such model of RTFM was favoured in many papers discussing magnetic characteristics of Ni:TiO_2 materials [22,23,26,31,33,35,38,39,42], the nature of RTFM in metal doped titanium dioxide still remains an open question.

3. EXPERIMENTAL

Water suspension of an industrial grade amorphous titanium dioxide (TiO_2/A) from sulphate technology supplied by "Chemical Factory Police S.A." (Poland) was used as a starting material. Commercial TiO_2 P25 (Evonik, Germany) was used for comparison. About 20 g of TiO_2 water suspension, containing ca. 35 wt.% of titanium dioxide and ca. 8 wt.% of residual sulfuric acid as related to TiO_2 content, was introduced into a beaker containing aqueous solution of $Ni(NO_3)_2$ and stirred for 48 h. The amount of Ni introduced to the beaker was of 1, 5 or 10 wt.% relative to TiO_2 content. These samples will be designated further as 1Ni,N-TiO_2, 5Ni,N-TiO_2, and 10Ni,N-TiO_2, respectively, or in short n=1, 5, and 10 wt.%. After water evaporation, samples were dried at 80 °C for 24 h in an oven. Subsequently, the material was calcined for 4 hours at 800 °C in NH_3 flow.

The phase composition of the obtained samples was investigated by XRD and is rather complex. In case of 1Ni,N-TiO_2 sample it is difficult to find any other phase than rutile. Thus, we have assumed that if any other crystalline phase is present in the

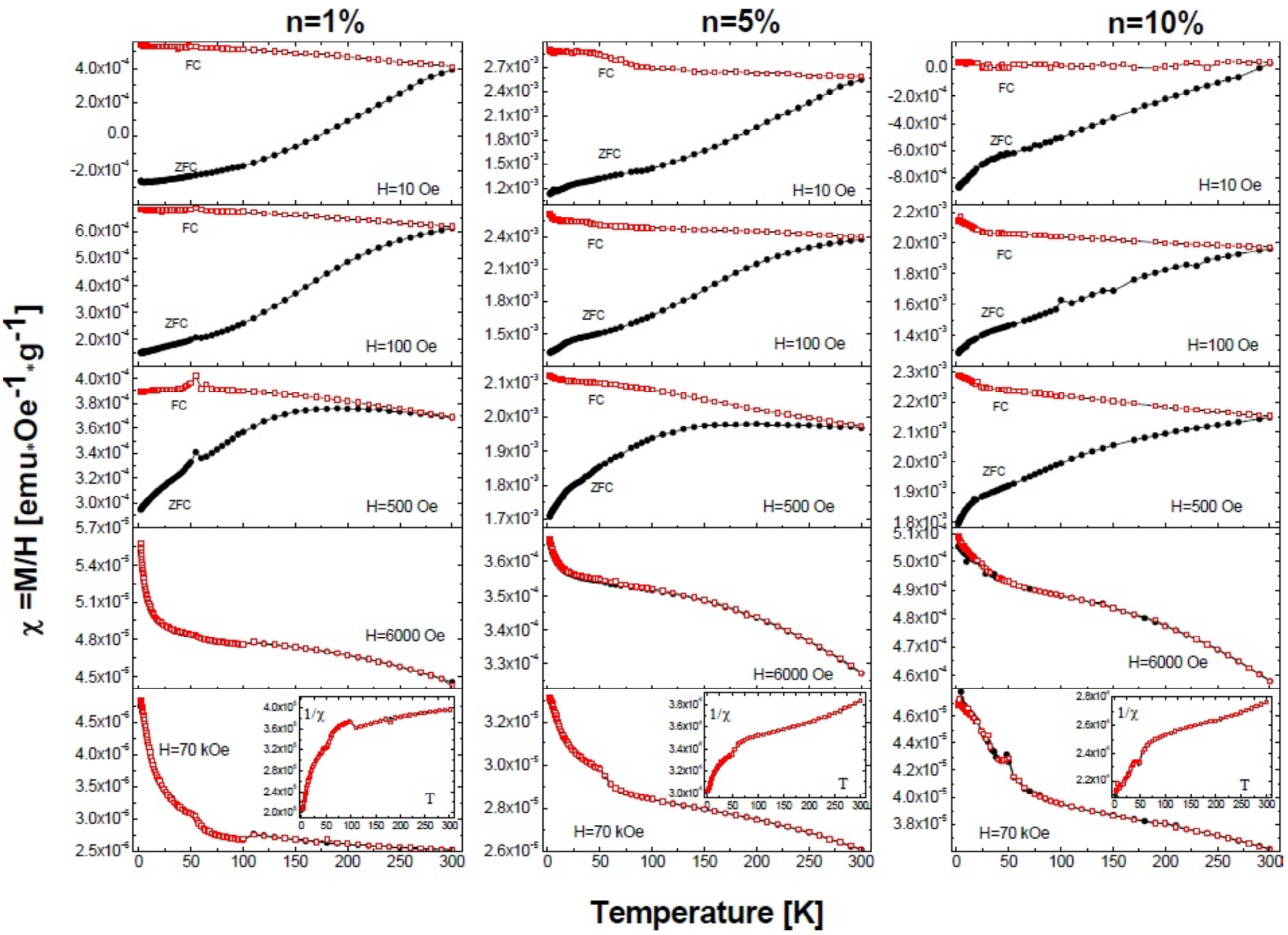

Fig. 1. Temperature dependence of the dc magnetic susceptibility χ of *n*Ni,N-TiO_2 samples in ZFC and FC modes in different applied magnetic fields *H*: (a) *n* = 1%, (b) *n* = 5%, and (c) *n* = 10%. The insets in the bottom row show the temperature dependence of the inverse magnetic susceptibility ($1/\chi$).

structure of 1Ni,N-TiO_2, its amount is negligible. In samples 5Ni,N-TiO_2 and 10Ni,N-TiO_2, a metallic nickel was detected. In sample 5Ni,N-TiO_2 also TiN phase appeared after the modification process.

DC magnetisation measurements (in ZFC and FC modes) were carried out by using a MPMS-7 SQUID magnetometer in the temperature range 2-300K and in magnetic field up to 70 kOe.

4. RESULTS AND DISCUSSION

Fig. 1 presents the temperature dependence of dc magnetic susceptibility χ (defined as $\chi = M/H$) in ZFC and FC modes of nickel and nitrogen co-modified TiO_2 nanocomposites, *n*Ni,N-TiO_2 (*n* = 1, 5, and 10 wt.%), registered at different external magnetic fields (*H* = 10, 100, 500, 6000, and 70000 Oe). All nanocomposites, independent on Ni concentration, exhibit a rather similar behavior. The ZFC and FC curves show temperature dependence of susceptibility which is typical for FM materials. As ZFC and FC branches of magnetic susceptibility, χ_{ZFC} and χ_{FC}, split at the temperature higher than RT, no SPM phase exists below RT and the Curie temperature must be accordingly much higher than 300K. In external fields smaller than ~1 kOe the χ_{FC} branch do not shows much temperature change when samples are cooled from RT down to 2K. On the other hand χ_{ZFC} branch decreases significantly on cooling the nanocomposites from RT. As the difference of the susceptibilities, χ_{FC}-$\chi_{ZFC,}$ is a measure of magnetic anisotropy it can be seen that in weak magnetic fields (below ~1 kOe) the anisotropy increases initially with the increase of Ni concentration (up to 5 wt.%), but for higher dopant content it remains constant. In external magnetic fields stronger than few kOe the χ_{ZFC} and χ_{FC} branches attain a similar thermal evolution and both branches are hard to discriminate. Temperature dependence of the susceptibility in strong magnetic fields, in the high temperature range (above ~100K), can be approximated with the Curie-Weiss law, producing a negative Curie-Weiss temperature indicative of an effective AFM interaction at high temperatures. In the low temperature range (below ~100K) that interaction weakens considerably and PM-type behavior is observed. It is interesting to notice that the strength of AFM interaction weakens also with in-

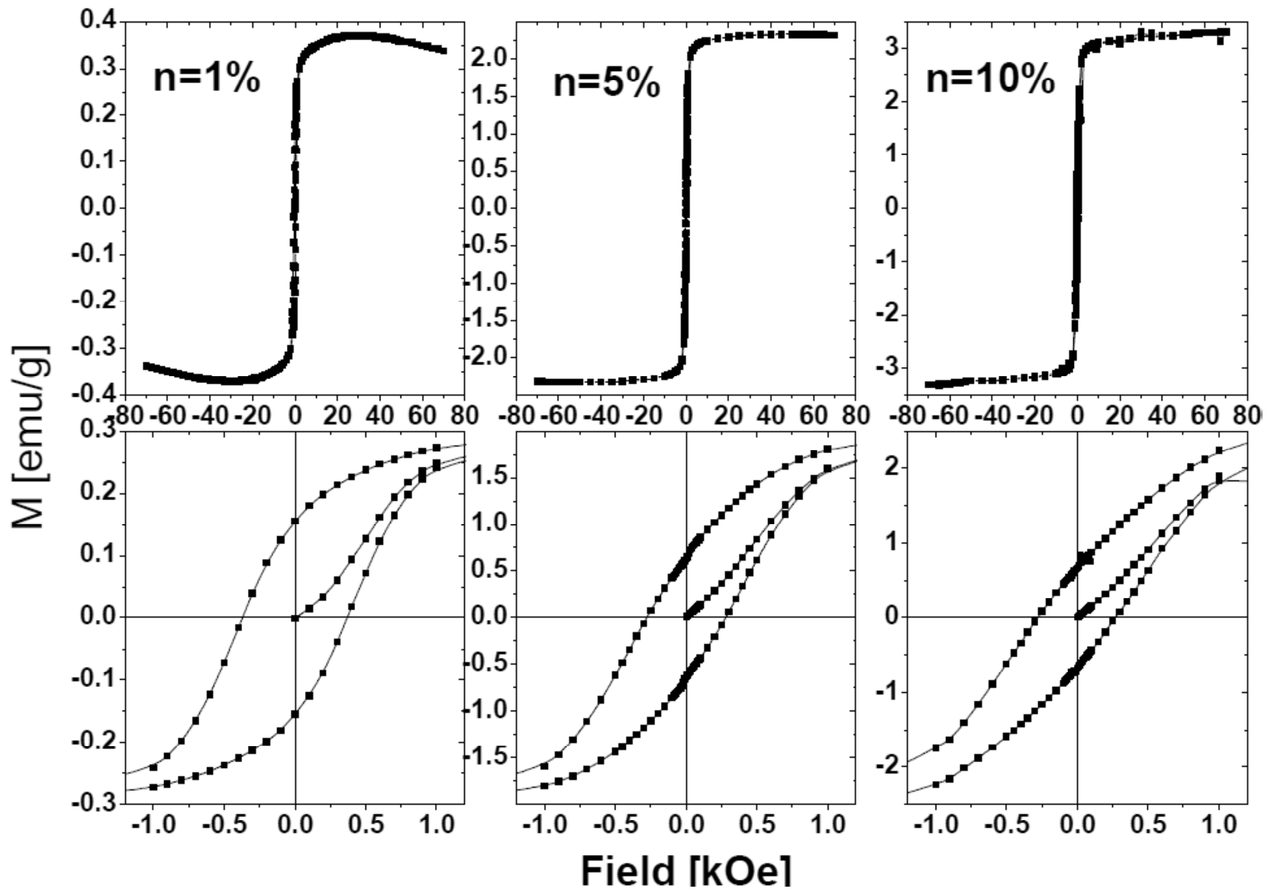

Fig. 2. Isothermal magnetisation at T = 2K of the three studied nanocomposites: (a) n = 1%, (b) n = 5% and (c) n = 10%. Bottom row shows magnified view of the central part of the registered hysteresis loops.

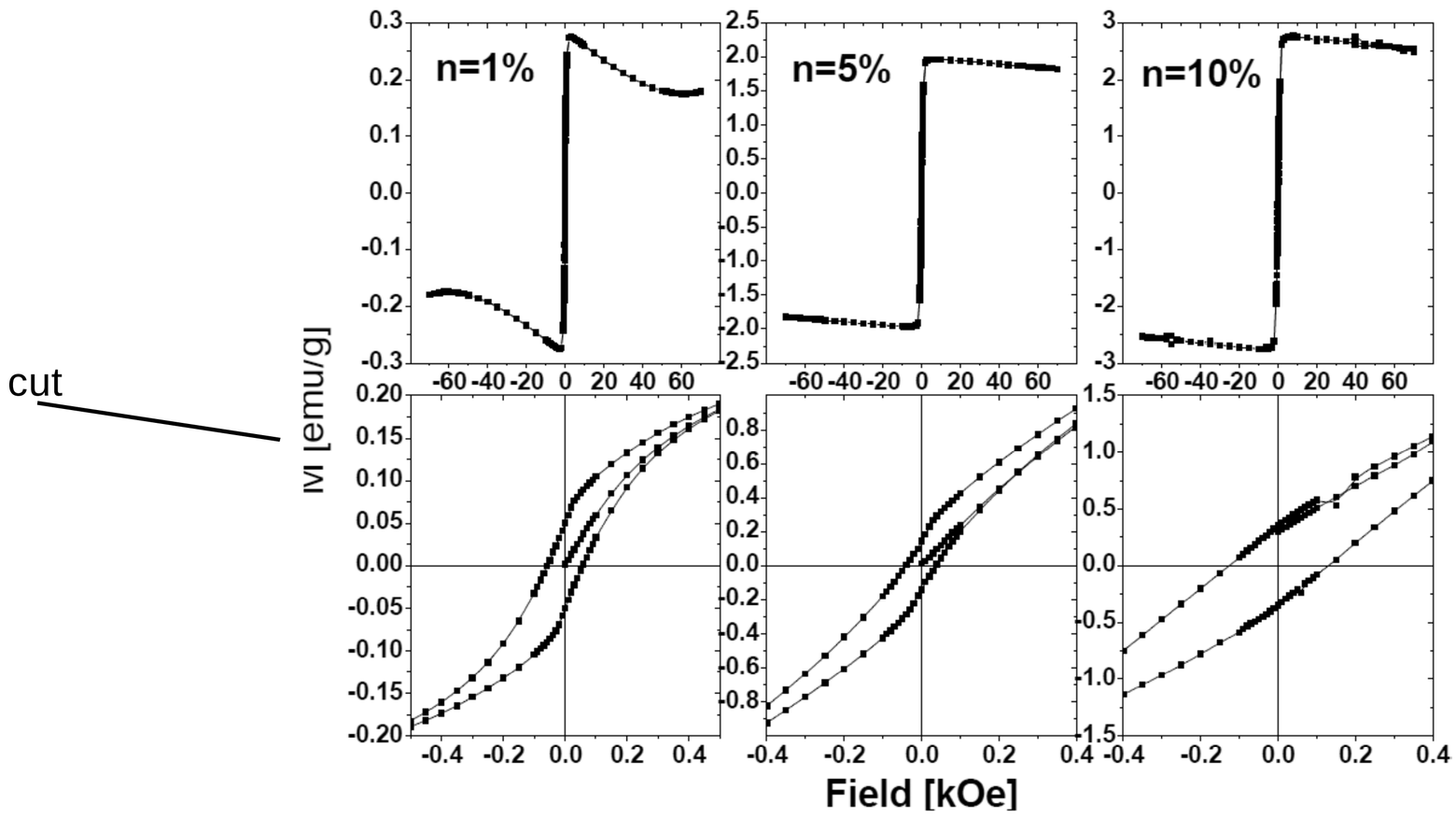

Fig. 3. Isothermal magnetisation at T = 300K of the three studied nanocomposites: (a) n = 1%, (b) n = 5% and (c) n = 10%. Bottom row shows magnified view of the central part of the registered hysteresis loops.

creasing concentration of nickel dopant. The temperature dependence of dc susceptibility presented in Fig. 1 for nNi,N-TiO_2 nanocomposites shows many similarities with what was previously registered for nFe,N-TiO_2 and nCo,N-TiO_2 [44,45]. It is very probable that a few magnetic components are present in nNi,N-TiO_2 nanocomposites producing a rather complicated magnetic response in an external magnetic field. Comparison of magnetic response of nNi,N-TiO_2 nanocomposites in low (H<1000 Oe) and in high (H~a few kOe and more) applied magnetic fields shows that many of these components are very weakly bounded magnetic entities that can be easily destroyed by not so strong external magnetic field. These magnetic centers might include different kinds of structural defects, involving nickel, titanium, nitrogen and oxygen atoms. They may be in form of magnetic clusters with both FM and AFM interactions.

In Figs. 2 and 3 the isothermal magnetisation registered at T = 2K and T = 300K of the three studied nanocomposites is shown. The magnetisation is rather small and magnetic loops are very narrow evidencing the presence of a rather weak FM at RT and at low temperature. The diamagnetic response of TiO_2 lattice (decreasing magnetisation with increasing magnetic field) is also clearly visible, for all samples at high temperature (300K) and for n = 1 wt.% sample at T = 2K. The three parameters characterizing the magnetic loop

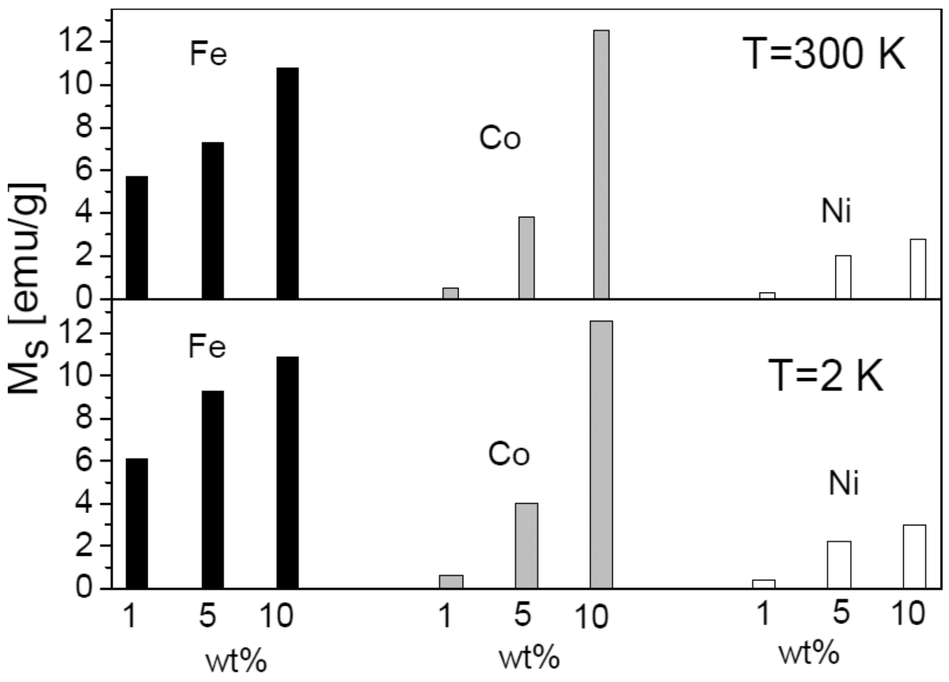

Fig. 4. Comparison of the saturation magnetisation M_s for Fe, Co and Ni doped and N co-doped TiO_2 nanoparticles measured at T = 300K (top panel) and 2K (bottom panel) for three different concentrations (1, 5, 10 wt.%) of doped 3d ions. Data of *n*Fe,N-TiO_2 nanocomposites is taken from Ref. 44, while for *n*Co,N-TiO_2 from Ref. 45.

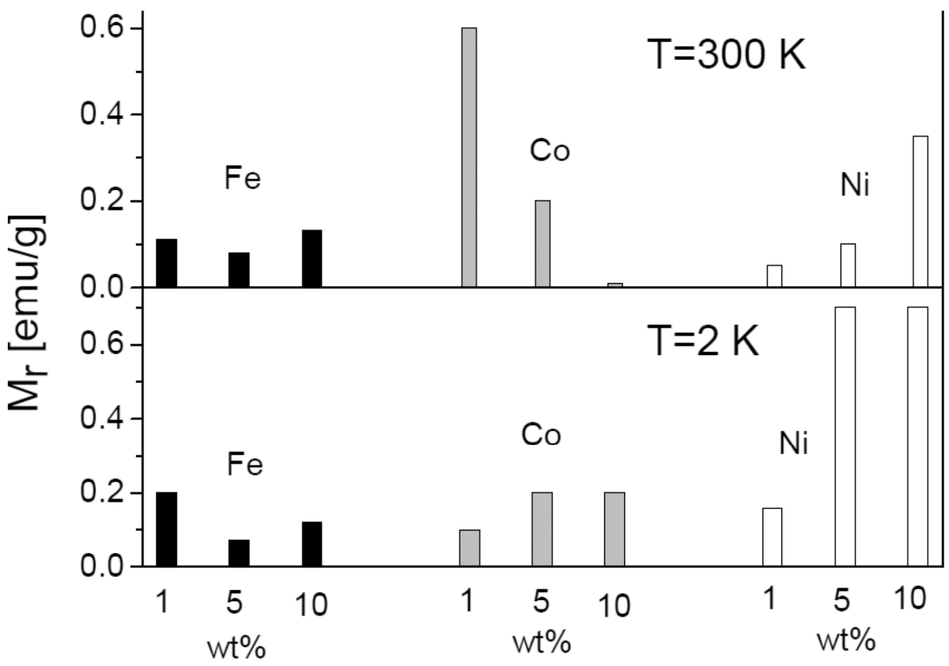

Fig. 5. Comparison of the remanent magnetisation M_r for Fe, Co, and Ni doped and N co-doped TiO_2 nanoparticles measured at T = 300K (top panel) and 2K (bottom panel) for three different concentrations (1, 5, 10 wt.%) of doped 3d ions. Data of *n*Fe,N-TiO_2 nanocomposites is taken from Ref. 44, while for *n*Co,N-TiO_2 from Ref. 45.

(saturation magnetisation M_s, remanent magnetisation M_r and the coercive field H_c) have been calculated for each sample and are presented in Figs. 4, 5, and 6. For comparison, the data of similar measurements on previously studied *n*Fe,N-TiO_2 and *n*Co,N-TiO_2 nanocomposites has been used and are shown in these figures [44,45].

The saturation magnetization M_s of *n*Ni,N-TiO_2 nanocomposites (Fig. 4) increases with concentration of Ni ions both at low (2K) and at high temperature (300K). Besides, M_s has similar values at these two temperatures in *n*Ni,N-TiO_2 samples. In comparison with the other two nanocomposites, *n*Ni,N-TiO_2 is generally magnetically weaker than *n*Fe,N-

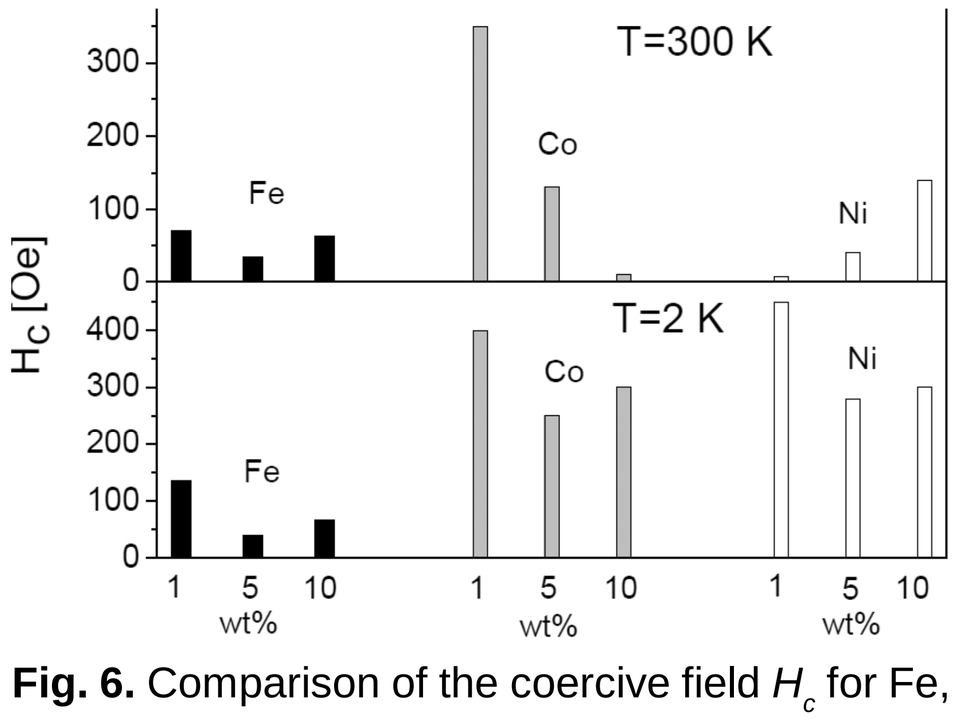

Fig. 6. Comparison of the coercive field H_c for Fe, Co, and Ni doped and N co-doped TiO_2 nanoparticles measured at T = 300K (top panel) and 2K (bottom panel) for three different concentrations (1, 5, 10 wt.%) of doped 3d ions. Data of *n*Fe,N-TiO_2 nanocomposites is taken from Ref. 44, while for *n*Co,N-TiO_2 from Ref. 45.

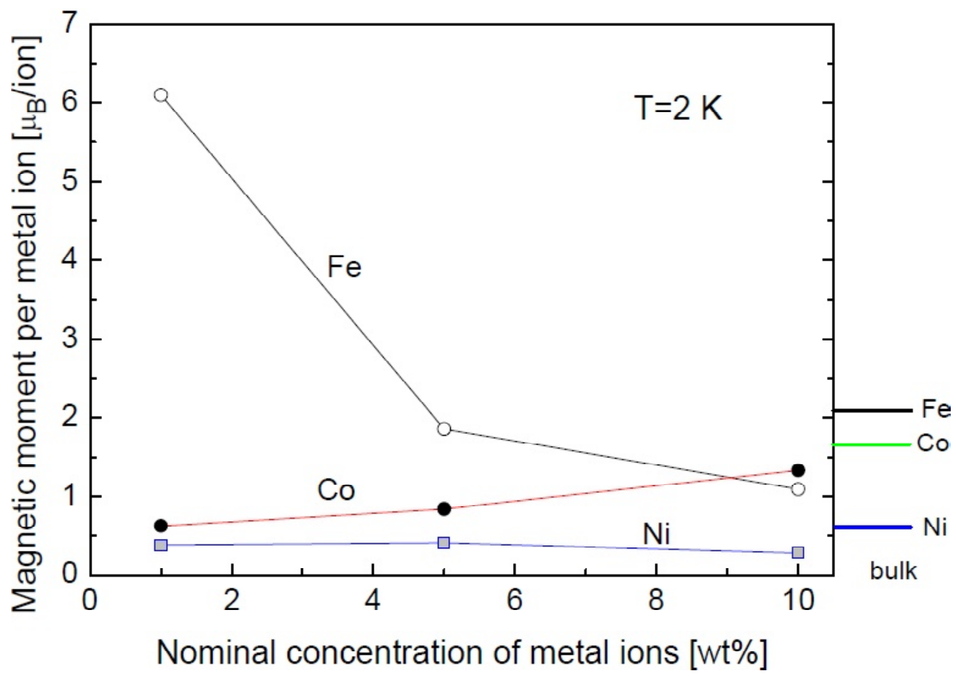

Fig. 7. Dependence of the magnetic moment per metal ion (Fe, Co, and Ni) on the nominal concentration of metal ions in TiO_2 nanocomposites. On the right-hand side the values of the magnetic moments in bulk metals are indicated.

TiO_2 and *n*Co,N-TiO_2. This is not unexpected as the spins of these three magnetic ions present in these nanocomposites are considered. Surprisingly, if only *n*=10 wt.% nanocomposites are taken into account, 10%Co,N-TiO_2 sample has the largest saturation magnetisation. It could mean that in the other two nanocomposites the AFM interactions are reducing their magnetism.

A different picture of magnetism in these nanocomposites emerges when the magnetic moment per a single doped magnetic ion is calculated from the saturation magnetisation (Fig. 7). Magnetic moment calculated on a single Ni atom is 0.38, 0.41, and 0.28 μ_B/Ni in n = 1 wt.%, 5 wt.%, and 10 wt.% nanocomposites at 2K, respectively. At 300K the moment is slightly smaller and equals 0.27, 0.38,

and 0.26 μ_B/Ni in 1 wt.%, 5 wt.%, and 10 wt.% samples, respectively. The tendency is easy to notice: magnetic moment increases initially with increasing nickel concentration, but for higher then 5 wt.% Ni content it decreases significantly. A similar trend was already observed in other Ni:TiO_2 samples [22]. It is interesting to compare these values with the saturation magnetisation in ferromagnetic bulk Ni which is equal to 0.61 μ_B/Ni. Thus the magnetic moment of a single Ni ion in our nanocomposites is not larger than 2/3 of the magnetic moment of Ni in a bulk metallic state. In *n*Fe,N-TiO_2 nanocomposites the magnetic moment on one Fe ion decreases with Fe concentration. This is in strong contrast to what is observed for *n*Co,N-TiO_2 nanocomposites – there the bigger Co content, the higher the magnetic moment of a single Co ion (Fig. 7). The obtained small values of Ni magnetic moment in *n*Ni,N-TiO_2 samples strongly indicate that the FM phase in these nanocomposites originates from external causes – metallic Ni inclusions. Besides, such metallic phase was already discovered in XRD study of our samples. Decrease of Ni magnetic moment in sample with high concentration of nickel (10Ni,N-TiO_2 nanocomposite) can be explained either by an increased amount of spurious phases (PM like $NiTiO_3$ or AFM like NiO) containing Ni atoms or be attributed to an increase in the AFM superexchange coupling strength between two neighboring Ni ions via a nearby O^{2-} ion in case of an intrinsic RTFM [22].

The remanent magnetisation (remanence) M_r of *n*Ni,N-TiO_2 nanocomposites at T = 300K increases with increasing concentration of Ni, but at T = 2K that increase saturates for n = 10 wt.% sample (Fig. 5). This behavior is quite the opposite of what is registered for *n*Co,N-TiO_2 samples. Here a decrease of remanence with increasing content of Co ions is observed. For the *n*Fe,N-TiO_2 nanocomposites, the dependence of M_r on Fe concentration is weak or absent and the n = 5 wt.% sample seems to have the smallest remanence.

The coercive field H_c of *n*Ni,N-TiO_2 samples at T = 300K increases with Ni content (similar as in the case of M_r), but at T = 300K this tendency is upset by a very large H_c of n = 1 wt.% sample (Fig. 6). The coercive field of *n*Co,N-TiO_2 samples seems to decrease with the concentration at both low and high temperatures, and at the later temperature this effect is quite impressive. There is no clear concentration dependence of the coercive field of *n*Fe,N-TiO_2 nanocomposites and the values of H_c for these samples are generally smaller than for *n*Co,N-TiO_2.

5. CONCLUSIONS

Review of papers dedicated to the study the magnetic properties of nickel doped titanium dioxide has shown that RTFM detected in most investigated samples can have two origins: external and internal. Because of a wide range of techniques that were used to synthesize samples, no single mechanism can explain RTFM in all Ni:TiO_2. In some cases FM was due to the nickel metal clusters or inclusions (an external cause), while in others a donor impurity band model which is an extension of the BMP model was successful in explaining RTFM (an internal cause). It was found that a large number of different factors during sample fabrication can have significant influence on its magnetic characteristics, including RTFM. Magnetisation measurements of three nickel and nitrogen co-modified titanium dioxide nanocomposites, *n*Ni,N-TiO_2 (n=1, 5, and 10 wt.%), has revealed a weak FM behaviour at RT and at lower temperatures that is mostly due to an external cause. Temperature dependence of dc susceptibility in ZFC and FC modes has indicated on the presence of a few magnetic components, including metallic nickel clusters and spurious phases. Comparison with previously studied similar systems, *n*Fe,N-TiO_2 and *n*Co,N-TiO_2 has shown that *n*Ni,N-TiO_2 nanocomposites displays a unique, very interesting magnetic characteristics.

ACKNOWLEDGEMENT

This work was partially supported by project Maestro 3, No. DEC-2012/06/A/ST5/00226 from the National Science Centre (Poland).

REFERENCES

[1] H.M. Yates, M.G. Nolan, D.W. Sheel and M.E. Pemble // *J. Photochem. Photobiol. A* **179** (2006) 213.
[2] T.L. Thompson and J.T. Yates Jr. // *Chem. Rev.* **106** (2006) 4428.
[3] K. Hashimoto, H. Irie and A. Fujishima // *Jpn. J. Appl. Phys*. **44** (2005) 8269.
[4] A.L. Stepanov // *Rev. Adv. Mater. Sci*. **30** (2012) 150.
[5] A. Zaleska // *Recent Pat. Eng*. **2** (2008) 157.
[6] Y. Matsumoto, M. Murakami, T. Shono, T. Hasegawa, T. Fukumura, M. Kawasaki, P. Ahmet, T. Chikyow, S. Koshihara and H. Koinuma // *Science* **291** (2001) 854.
[7] T. Dietl, H. Ohno, F. Matsukura, J. Cibert and D. Ferrand // *Science* **287** (2000) 1019.

[8] K. Sato and H. Katayama-Yoshida // *Jpn. J. Appl. Phys.* **39** (2000) L555
[9] D.P. Norton, S.J. Pearton, J.M. Zavada, W.M. Chen and I.A. Bouyanova, In: *Zinc Oxide Bulk, Thin Films, and Nanostructures*, ed. by C. Jagadish and S.J. Pearton (Elsevier: New York, 2006), p. 555.
[10] J.M.D. Coey, M. Venkatesan and C.B. Fitzgerald // *Nat. Mater*. **4** (2005) 173.
[11] R. Janisch, P. Gopal and N.A. Spaldin // *J. Phys.: Condens. Matte*r **17** (2005) R657.
[12] X.L. Li, S.F. Qi, F.X. Jiang, Z.Y. Quan and X.H. Xu // *Sci. China-Phys. Mech. Astron*. **56** (2013) 111.
[13] J.K. Furdyna, S. Lee, M. Dobrowolska, T. Wojtowicz and X. Liu, In: *Introduction to the Physics of Diluted Magnetic Semiconductors*, ed. by J. Kossut and J.A. Gaj (Springer-Verlag: Berlin, Heidelberg, 2010), p.103
[14] K. Yates, In: *Nanomagnetism and spintronics*, ed. by F. Nasirpouri and A. Nogaret (World Scientific: Singapore, 2011), p. 223
[15] N.H. Hong, W. Prellier, J. Sakai and A. Hassini // *Appl. Phys. Lett.* **84** (2004) 2850.
[16] X.T. Zu, S. Zhu, X. Xiang and L.M. Wang // *Microsc. Microanal.* **11** (2005) 1906.
[17] N.H. Hong, J. Sakai, W. Prellier and A. Ruyter // *J. Phys. D: Appl. Phys*. **38** (2005) 816.
[18] J.V. Pinto, M.M. Cruz, R.C. da Silva, E. Alves and M. Godinho // *J. Magn. Magn. Mater.* **294** (2005) e73.
[19] S. Zhu, L. M. Wang, X. T. Zu and X. Xiang // *Appl. Phys. Lett.* **88** (2006) 043107.
[20] L. Sangaletti, M.C. Mozzati, P. Galinetto, C.B. Azzoni, A. Speghini, M. Bettinelli and G. Calestani // *J. Phys.: Condens. Matter* **18** (2006) 7643.
[21] N. Shimizu, K. Yamaki, T. Mochiku, K. Yamada, S. Itoh and K. Kadowaki // *phys. stat. sol. (c)* **3** (2006) 4151.
[22] Y.R. Park, S.L. Choi, J.H. Lee and K.J. Kim // *J. Korean Phys. Soc*. **50** (2007) 638.
[23] D.L. Hou, H.J. Men, L.Y. Jia, X.J. Ye, H.J. Zhou and X.L. Li // *Phys. Lett. A* **364** (2007) 318.
[24] A.F. Cabrera, L. Errico, C.E. Rodrýguez Torres and F.H. Sanchez // *Physica B* **389** (2007) 103.
[25] M.C. Mozzati, P. Galinetto, C.B. Azzoni, L. Sangaletti, A. Speghini and M. Bettinelli // *phys. stat. sol. (c)* **4** (2007) 1264.
[26] J. Chen, G.H. Lu, H. Cao, T. Wang and Y. Xu // *Appl. Phys. Lett.* **93** (2008) 172504.
[27] H.Y. Zhang, T.H. Ji, L.L. Li., X.Y. Qi, Y.F. Liu, J.W. Cai, H.Y. Du and J.Y. Sun // *Acta Phys. Chim. Sin.* **24** (2008) 607.
[28] H. Peng, J. Li, S.S. Li and J.B. Xia // *J. Phys.: Condens. Matter* **20** (2008) 125207.
[29] B.F. Ding, Y.P. Li and L.M. Wang // *Chin. Phys. Lett.* **28** (2011) 107802.
[30] M. Karimipour, J.M. Wikberg, V. Kapaklis, N. Shahtahmasebi, M.R.R. Abad, M. Yeganeh, M.M. Bagheri-Mohagheghi and P. Svedlindh // *Phys. Scr*. **84** (2011) 035702.
[31] N. Bahadur, R. Pasricha, Govind, S. Chand and R.K. Kotnala // *Mater. Chem. Phys.* **133** (2012) 471.
[32] Y.L. Zhao, M. Motapothula, N.L. Yakovlev, Z.Q. Liu, S. Dhar, A. Rusydi, Ariando, M.B.H. Breese, Q. Wang and T. Venkatesan // *Appl. Phys. Lett.* **101** (2012) 142105.
[33] J. Tian, H. Gao, H. Deng, L. Sun, H. Kong, P. Yang and J. Chu // *J. Alloy. Compd.* **581** (2013) 318.
[34] N.T.O. Hoa and D.N. Huyen // *J. Mater. Sci.: Mater. Electron*. **24** (2013) 793.
[35] J. Tian, H. Gao, H. Kong, P. Yang, W. Zhan and J. Chu // *Nanoscale Res. Lett*. **8** (2013) 533.
[36] X.W. Wang, X.T. Shi, S.P. Lv, J. Chen and S.Y. Wang // *Adv. Mat. Res.* **668** (2013) 723.
[37] W.Ch. Chiang, W.L. Lan, Y.-H. Tang and J.G. Lin // I*EEE T. Magn.* **50** (2014) 1000804.
[38] M. Vranjes, Z. Konstantinovic, A. Pomar, J. Kuljanin Jakovljevic, M. Stoiljkovic, J.M. Nedeljkovic and Z. Saponjic // *J. Alloy. Compd*. **589** (2014) 42.
[39] J. Yuh and W.M. Sigmund // *J. Ceram. Process. Res*. **16** (2015) 93.
[40] Q. Wang, X. Liu, X. Wei, J. Dai and W. Li // *J. Nanomater.* **2015** (2015) 371582.
[41] N. Guskos, G. Zolnierkiwicz, A. Guskos, J. Typek, P. Berczynski, D. Dolat, S. Mozia and A.W. Morawski, In: *NATO Science for Peace and Security Series C: Environmental Security, Nanotechnology in the Security Systems*, ed. by. J. Bonca and S. Kruchinin (Springer Science+Business Media: Dordrecht, 2015), pp. 33.
[42] M. Esakkimuthuraju, R. Mahesh, T. Sreekanth and P. Venugopal Reddy // *Proc. SPIE* **9364** (2015) 93641N.

[43] M.V. Ganduglia-Pirovano, A. Hofmann and J. Sauer // *Surf. Sci. Rep.* **62** (2007) 219.
[44] N. Guskos, S. Glenis, G. Zolnierkiwicz, A. Guskos, J. Typek, P. Berczynski, D. Dolat, S. Mozia and A.W. Morawski // *Open Phys*. **13** (2015) 78.
[45] N. Guskos, J. Typek, G. Zolnierkiewicz, A. Diamantopoulou, S. Mozia and A.W. Morawski, to be published In: *NATO Science for Peace and Security Series A: Chemistry and Biology*, ed. by. J. Bonca and S. Kruchinin, 2016.